Cancer Letters 448 (2019) 1–10

Contents lists available at ScienceDirect

Cancer Letters

journal homepage: www.elsevier.com/locate/canlet

Original Articles

Nanoliposomal formulation encapsulating celecoxib and genistein inhibiting COX-2 pathway and Glut-1 receptors to prevent prostate cancer cell proliferation

Jingyan Tian[a], Fengjun Guo[b], Yingying Chen[a], Yanqing Li[a], Bingbing Yu[a], Yang Li[a,*]

[a] Department of Pathophysiology, College of Basic Medical Sciences, Jilin University, 126 Xinmin Street, Changchun, 130021, Jilin, PR China
[b] Department of Gynaecology and Obstetrics, The Second Hospital of Jinlin University, 218 Ziqiang Street, Changchun, 130041, Jilin, PR China

ARTICLE INFO

Keywords:
Nanoliposomes
Drug delivery
Genistein
Celecoxib
Prostate cancer

ABSTRACT

Globally, prostate cancer remains a challenging health burden for men as it is the second leading cause of cancer death in men and about one in nine will be diagnosed with prostate cancer in his lifetime. Enhanced expression of COX-2 and Glut-1 proteins are reported as major factors leading to the origin and progress of prostate cancer through modulating the associated signaling pathways. In this study, we have synthesized a multifunctional liposomal system containing celecoxib and genistein drugs. The combinatorial effect of these drugs leads to the selectively induce the apoptosis of prostate cancer cells than normal fibroblast cells. The mechanistic study suggests that enhanced reactive oxygen species (ROS) formation and a decrease in cellular GSH concentration, along with inhibition of COX-2 synthesis and Glut-1 receptors are the key processes behind the inhibition of prostate cancer cells. Overall, these results provide strong evidence for the role of COX-2 and Glut-1 proteins for the progression of prostate cancer and highlighting the potential of celecoxib and genistein as a useful and combinatorial pharmacological agent for chemotherapeutic purposes in prostate cancer.

1. Introduction

Although there has been tremendous progress in the development of novel strategies for prostate cancer treatment, however, it still remains as one of the most challenging health burdens for men globally. As per the statistics of the year 2012, there were over 1 million new prostate cancer patients, accounting for 8% of all the new cancer cases worldwide [1]. In recent past, there has been a significant development in the realm of molecular biology, immunology, and target identification, which have produced a rich library of new targets, signaling pathways, and antibodies for immunotherapies. Additionally, investigations in the domain of new drug development have led to the identification of novel anticancer drugs. However, despite utilizing these tools, the successful handling of prostate cancer has not been realized so far. Although it is well known that the possible major obstacle is the early detection of prostate cancer biomarkers, however, target-dependent delivery of anticancer agents remains at the top of the list.

Among several anticancer drugs developed for inhibition of prostate cancer progression, celecoxib is one of the key drug types, which has shown excellent results in several studies [2–7]. Celecoxib is a cyclooxygenase (COX-2) dependent nonsteroidal anti-inflammatory drug (NSAID) generally prescribed to reduce pain and inflammation. As an inducible enzyme, COX-2 modulates the production of prostaglandin E2 and thus reported to be overexpressed in different types of cancers including breast, colon, lung, melanoma, and prostate [2,3]. In prostate cancer cells, COX-2 has been considered as a key target, which plays an important role in the development of 50–70% of prostate tumors [8,9]. Celecoxib is known to inhibit COX-2 expression, which leads to the reduction in the cellular prostaglandin E2 leading to the compensatory increase in COX-2 protein concentration in cells [2,10]. The role of prostaglandin E2 has been linked with proliferation, invasiveness, angiogenesis, avoiding apoptosis, and production of tumor-inducing eicosanoids [11,12]. Further, it has been reported that in human studies the effect of celecoxib is limited, which could be due to its efficacy variation from androgen dependence to independence. A study reported by Zheng et al. revealed that the xenografted tumors generated from androgen-dependent LNCaP cells, upon treatment with celecoxib, regressed initially, however, tumors eventually progressed androgen dependence and thus started to develop further [13]. Despite the broad spectrum use of celecoxib in many cancer types, its administration is limited due to the safety concerns, potentially to serious toxicity to healthy individuals including increased risk of cardiovascular events

* Corresponding author.
E-mail address: yli1981@yahoo.com (Y. Li).

https://doi.org/10.1016/j.canlet.2019.01.002
Received 13 November 2018; Received in revised form 18 December 2018; Accepted 8 January 2019
0304-3835/ © 2019 Published by Elsevier B.V.

including myocardial infarction [14,15]. When compared with other NSAID, celecoxib, at dosages greater than suggested clinically, showed a lower incidence of symptomatic ulcers and related complications along with other clinically important toxic effects [16]. Therefore, it may be suggested to use the lowest possible concentrations of celecoxib for prostate cancer treatment.

It is well documented that cancer cells have rapid metabolism with high glucose consumption to fuel the metabolism. Considering this characteristic, cancer tissues are imaged by PET (Positron Emission Tomography), where a radiolabelled (^{18}F)-2-Fluoro-2-deoxy-D-glucose (FDG) is used. This glucose analog is rapidly taken up by cancer cells, which are identified using radioactive signals. The rapid glucose transport in cancer cells is facilitated by glucose transporter (Glut) proteins, spanning across the cell membrane. Although there are several types of Glut proteins, Glut-1 proteins have been considered to be involved in glucose transport among cancer cell membrane. Further, to investigate the role of Glut-1 receptors over glucose uptake, Singh et al. [17] have developed two types of gold nanoclusters coated with BSA and glucose and followed the pattern of internalization of these probes in cancerous and noncancerous skin cells. They reported that glucose coated nanoclusters were not taken up by noncancerous (HaCaT) cells, however, specifically taken up by cancerous (A431) cells through Glut-1 receptors. It was also found that the uptake of glucose coated nanoclusters was cell membrane potential independent while BSA coated nanoclusters were found internalize by membrane potential dependent manner. Studies involving humans suggest that high levels of Glut-1 expression in tumors are associated with poor survival [18]. Hypoxia is also reported to increase Glut-1 levels and thus glucose uptake. Further, Chandler et al. have reported that Glut-1 receptors are highly expressed in human prostate cancer cells and are associated with the Golgi body, possibly offering glucose supply to Golgi for by-product incorporation into the prostate secretion [19]. Thus targeting Glut-1 could be a novel strategy for detection and treatment of prostate cancer. Genistein is a well-known inhibitor of the Glut-1 protein, and thus induce the formation of ROS and association with AMPK signaling pathway activation. Considering the above discussion, genistein could be considered as a novel chemotherapeutic agent for prostate cancers. Although genistein alone may not be able to induce significant suppression to prostate cancer progression, however, combined with some known anti-prostate cancer agent could offer excellent results. Hwang et al. have reported that genistein combined with 5-Fluorouracil can effectively inhibit the progression of colon cancer cells, where genistein acts as cell sensitizer supporting 5-Fluorouracil to abolish the up-regulated COX-2 and prostaglandin secretion [20].

Traditional methods of cancer treatment involve single anticancer agent prescribed to patients and that have realized to have limited success due to the toxicity to healthy cells and resistance to cancer cells. Such obstacles are more pronounced due to the administration of a high dose of anticancer agents in order to achieve enhanced efficacy. A well-known example is a use of Vemurafenib (PLX4032) for the treatment of melanoma. Although the drug showed excellent melanoma regression activity, however, the long-term use eventually led to the resistance in melanoma cells [21]. Further investigation revealed that repeated exposure of a drug led to the development of an alternative survival pathway and thus express suitable cell surface receptors. Such events are common in the strategies involving single drug treatment because targeting individual signaling pathway of cancer cell survival may not be enough to achieve high therapeutic efficacy. Owing to the multigene abnormality, the survival of cancer cells is regulated by multiple signaling pathways, therefore, formulations containing multiple drugs (targeting multiple pathways) could be the strategy for cancer treatment with better results.

Nanomaterials, such as nanoliposomes, micelles, polymeric, metallic, and other nanostructures, have shown excellent results in encapsulating multiple anticancer agents and delivering them at the desired tumor site [22–26]. Nanomaterials-based drug delivery agents also offer the controlled release of drugs in the desired ratio and long-term circulation in the blood, which further enhances the treatment efficacy. Drug delivering nanocarriers offer better therapeutic efficacy due to the “Enhanced Permeable and Retention” (EPR) effect exhibited by nanomaterials of ~100 nm diameter. This passive targeting is mainly facilitated by leaky vasculature in cancer tissues, which unlike normal healthy vessels, have ~600–800 nm wide gaps among adjacent endothelial cells. Such faulty vascular system with poor lymphatic drainage enables drug delivering nanomaterials to extravasate into the extravascular space and accumulate in tumor tissues [27,28]. It has been reported that due to EPR effect ~10 fold increase in drug retention occurs in tumor region compared to free drugs [29]. PEGylation (stealthing) of the nanoparticles are suggested to make them “invisible” to the macrophages and phagocytes leading to the long circulation time in blood [30,31].

Approaches using co-delivery strategy for prostate cancer treatment are limited and have used non-specific drugs. Patil et al. have reported the co-encapsulation of mitomycin C and doxorubicin in liposome conjugated with folate receptors. This formulation showed enhanced toxicity to LNCaP prostate cancer cell line and KB cells [32,33]. Another study reported the use of a combination of doxorubicin and chloroquine (as chemosensitizer). Their result showed that the prostate tumor growth was arrested during the three-week administration period without any pervasive side effects [34]. Recently, there have been increasing attention towards the development of multifunctional nanocarriers which can combinatorially deliver the chemotherapeutic agents and produce maximum therapeutic efficiency. Such strategies using selected drugs can overcome multidrug resistance as well as inhibit the anti-apoptotic property of cancer cells and achieve synergistic anticancer effects.

In this work, we report the synthesis of a multifunctional liposome-based nanocarrier system encapsulating celecoxib and genistein. The prostate cancer cell-based assays suggest the inhibition of proliferation of cancer cells and no effect to normal fibroblasts cells. The mechanistic investigation revealed that both of these drugs deregulate the key signaling pathways of prostate cancer cells needed for their growth and metastasis. Inhibition of the expression of COX-2 and Glut-1 receptors thereby decreased glucose intake were some of the vital processes, which induce the prostate cancer cell apoptosis.

2. Materials and experimental methods

2.1. Preparation of liposomes containing celecoxib and genistein

The synthesis of nanoliposomes was performed by following a method described by Gowda et al. [25] with slight modification. Briefly, the liposomes were prepared by using L-α-phosphatidylcholine (eggPC) and 1,2-dipalmitoyl-sn-glycero-3-phosphoethanolamine-N-[methoxy(polyethylene glycol)-2000] ammonium salt (DPPE-PEG-2000) in chloroform at 95:5 mol % with 25 mg/mL total lipid concentration (Avanti Polar Lipids). Chloroform from the lipid mixture was removed by blowing N_2 gas and the so obtained lipid film was suspended in sterile saline solution or water with intermittent vortexing at 60 °C. This process was continued for about 30 min, followed by sonication and extrusion through a 100 nm polycarbonate membrane at 60 °C using Avanti Mini-Extruder (Avanti Polar Lipids). The above-mentioned process was used to prepare empty liposomes (EL). The liposomes encapsulating celecoxib (CL), genistein (GL) and celecoxib with genistein (CGL) were also followed the same preparation process except for the drugs (celecoxib with genistein) were mixed with lipids during the drying process.

2.2. Physicochemical characterization of liposomes

Zeta potential and hydrodynamic size of above-prepared liposomes were estimated using Dynamic Light Scattering (DLS) (Zeta sizer nano,

Malvern Instruments, Malvern, United Kingdom) operating with a laser of 633 nm wavelength. Typically, 50 μL of different liposomes (EL, CL, GL, and CGL) were suspended in 950 μL of Milli-Q water followed by gentle vortexing. The resultant suspension by used for zeta potential and hydrodynamic size measurement. The size and shape of liposomes were also measured by transmission electron microscope (TEM) (JEOL JEM1400), by negatively staining of the liposomes. Briefly, different liposomes were drop casted on a Cu-coated TEM grid followed by overnight drying at ambient conditions. For negative staining of liposomes, 10 μL of uranyl acetate was flushed on liposome containing TEM grid for 45 s. Next, the stained liposomes were gently washed with excess of deionized water followed by drying in a desiccator for 6 h (uranyl acetate was diluted with 1:3 ratio using deionized water).

2.3. Drug encapsulation and release kinetics

Encapsulation of celecoxib and genistein drugs, either alone or in combination (10:1 ratio) in liposomes was determined by UV–Visible spectrophotometer. In order to remove the un-incorporated drugs from the prepared liposomes were removed by centrifugation (4000 rpm, 15 min) of liposomes with 10 kDa Amicon filter tube (Millipore). Further, 1 mL of separated liposomes were mixed with an equal volume of chloroform and methanol followed by vigorous vortexing. This process breaks the liposomes and thus release the encapsulated drugs in the solution. Further, the lipid molecules are separated by centrifuging the suspension at 10,000 rpm for 30 min. The so obtained supernatant was used for the estimation of celecoxib, genistein drug concentration encapsulated in liposomes either alone or in combination. To obtain the accurate concentration of drugs, a standard curve of both the drugs were also made ranging from 0.01 to 1 mg/mL. Drug encapsulation percentage was calculated as the free drug(s)/total drug (s) X 100. To quantitatively estimate the release kinetics of the encapsulated drugs, the representative liposomes were dialyzed at room temperature using a 25 kDa molecular weight cutoff cellulosic dialysis membrane. A 5 mL of liposomal suspension was placed in the dialysis membrane which was placed in saline or water (1 L) containing 10 mM glutathione. A sample of 50 μL of liposome was removed from the dialysis bag at different time intervals and upon digestion of liposomes (method described above), the released amount of respective drugs were monitored by UV–vis spectrophotometer.

2.4. Assessment of prostate cancer cell viability

Typically, in a 96-well plate prostate cancer cell culture models (PC-3 and LNCaP cells) and normal fibroblasts (FF2441) were seeded (1×10^4 cells/well) and incubated overnight. Each cell lines were exposed with EL (control), CL (100 μM), GL (10 μM), and CGL (100 μM celecoxib and 10 μM genistein) for 24, 48, and 72 h followed by cell viability assessment using MTT assay method. The developed formazan crystals were solubilized in 100 μL of DMSO followed by cell viability estimation by measuring the absorbance at 590 nm in a multi-well plate reader.

2.5. Cell migration assay

In a 6-well cell culture plate, about 2×10^6 PC-3 cells were seeded and incubated overnight. Using a 1 mL pipette tip, a linear scratch was created across the cell monolayer in each well. After creating the scratch, the cell monolayer was washed with the cell culture media to remove the scratched cells and cell debris. Next, the cells were treated with EL (control), CL (100 μM), GL (10 μM), and CGL (100 μM celecoxib and 10 μM genistein) for 24 and 48 h followed by image acquisition.

2.6. ROS generation assay

A fluorescence dye (H_2DCFDA, 2, 7-dichlorofluorescein diacetate) was used to estimate the produced ROS in PC-3 and LNCaP and fibroblast cell culture models. These cells (1.0×10^4) were seeded in a black bottom 96-well plate followed by 24 h of incubation. Cells were treated with different liposomal formulations for EL (control), CL (100 μM), GL (10 μM), and CGL (100 μM celecoxib and 10 μM genistein) 48 h. After the exposure period, media was discarded and cells were washed twice with PBS followed by addition of 100 μL of H_2DCFDA dye (20 μM) in each well and incubated for another 30 min at 37 °C under dark condition. Finally, the dye solution was removed and cells were washed twice with PBS followed by fluorescence intensity (Ex/Em = 485 and 528 nm) measurement from each well using a multiwell plate reader.

2.7. Glutathione estimation

The GSH concentration was estimated by using Glutathione estimation kit (Cayman, 703002) and the obtained quantity was expressed as μmole/mg of protein. Briefly, 2.0×10^5 cells/well were seeded in a 6 well cell culture plate followed by overnight incubation. Next, cells were exposed to EL (control), CL (100 μM), GL (10 μM), and CGL (100 μM celecoxib and 10 μM genistein) for 24 h. Further, the cells were washed twice with PBS followed by scraping and collection in 0.5 mL MES buffer already included in the kit. Next, cells were sonicated for 5 min (10 s 'on', 5 s' off') at 30% amplitude in iced MES buffer followed by centrifugation (11,000 g at 4 °C for 20 min). The so obtained supernatant containing GSH was used for quantitative estimation. A 50 μL volume of the so obtained supernatant from each sample was taken in a separate 96 well plate followed by addition of 150 μL of the reaction mixture [cofactor mixture, enzyme mixture, 5,5′-dithiobis-(2-nitrobenzoic acid) (DTNB)]. Next, the plate was incubated for 30 min in dark at room temperature and finally, the absorbance of the reaction mixture was recorded at 405 nm using a spectrophotometer. Protein concentration in each sample was quantified by the Bradford assay.

2.8. Glucose uptake estimation

The glucose uptake in cells was measured by considering a fluorescent analog (2-NBDG) of glucose. About 2.0×10^5 cells/well were seeded in a 6 well cell culture plate and incubated for 24 h. Further, the cells were exposed to different liposomal formulations for 24 h. Next, the media was removed and cells were washed twice with PBS. Next, cells were incubated with PBS solubilized NBDG (1 mL, 100 μM) at 37 °C for 20 min. Upon incubation, the NBDG solution was removed and cells were washed twice with PBS followed by trypsinization and recovery of cells. The so obtained cell pellet was washed again with PBS and finally suspended in 0.5 mL of PBS. The result was acquired using flow cytometer under the green channel to obtain the signatures of 2-NBDG in cells.

2.9. Western blotting

In a 6 well cell culture plate, about 2.0×10^6 cells/well were seeded and incubated overnight. Next day, the cells were exposed to EL (control), CL (100 μM), GL (10 μM), and CGL (100 μM celecoxib and 10 μM genistein) for 24 h. Next, the cells were washed twice with PBS followed by lysis with (200 μL) of CelLytic MT cell lysis reagent (Sigma). Further, the cells were broken down by sonication at 25% amplitude (10 s 'on', 5 s 'off') for 3 min followed by centrifugation at 12000 rpm for 25 min the so obtained supernatant was isolated and the concentration of protein for each sample was quantified by the Bradford assay. A 12% SDS polyacrylamide gel electrophoresis (PAGE) was considered to resolve the isolated protein (25 μg) and later transferred onto a polyvinylidene difluoride (PVDF) membrane using 300 mV for 2 h. The protein containing membrane was blocked by using 5% skim milk dissolved in TBST (tween-tris buffer saline) buffer for 3 h followed by washing thrice using TBST (10 min wash cycle). The blot was further incubated with protein-specific primary antibodies (Abcam, Cambridge,

UK) [GAPDH, COX-2, Glut-1, TrxR, Prx-6, and Cleaved caspase-3) in a 1:2000 dilution in TBST and the antibodies are incubated overnight at 4 °C. Next, the blot was washed thrice with TBST followed by incubation with the suitable secondary antibody (1:5000 dilution) for 3 h. Finally, the blot was washed thrice with TBST and developed using chemiluminescence (Super Signal West Femto chemiluminescent reagent, Pierce, Rockford, IL) and analysed through ImageQuant LAS500 software (GE Healthcare Bio-Sciences AB, Sweden). Finally, the obtained protein bands were quantified by using densitometry analysis using Image-J.

2.10. Real-time polymerase chain reaction

About 2.0×10^5 cells were seeded in a 6 well cell culture plate followed by incubation for 24 h. Next, the cells were treated with different liposomal formulations for 24 h. Next, the culture media was aspired followed by washing of cells with PBS. The Trizol method was used for isolation of total RNA from the treated cells. A 500 μL of Trizol reagent was mixed with cells followed by addition of 100 μL of chilled chloroform. This mixture was vortexed and mixed followed by centrifugation at 12000*g* for 20 min at 4 °C. The so obtained three layers were seen and the clear aqueous layer containing RNA was isolated and quantified by UV–Visible spectrophotometer by following the absorbance at 260 nm. The cDNA was synthesized by using a cDNA synthesis kit (Thermofisher). The purified RNA (0.5 μg) was taken as a template and the genes of interest were amplified using specific primer sets with SYBER green dye. A 20 μL of PCR reaction containing cDNA template (2 μL), SYBR green dye (10 μL) and gene-specific primers (1 μL each of forward and reverse primers) (COX-2, Glut-1, TrxR, Prx-6, and Cleaved caspase-3) and experiment was performed using Quant qRT-PCR (QuantStudio™ 5 System, Thermofischer). The program details are as follows, 95 °C, 10 min, followed by 95 °C, 15 s; 60 °C, 30 s; 72 °C, 30 s (40 cycles). The relative expression levels of each gene were calculated considering comparative CT values. The CT value of the gene was normalized with the CT value of GAPDH considering its intensity remains constant in treated cells than untreated control cells.

3. Results and discussion

3.1. Synthesis and characterization of nanoliposomes encapsulating celecoxib and genistein

Recently, liposomes-based nanoparticles (nanoliposomes) have shown tremendous success towards improved therapies including delivery of therapeutic drugs/genes at the targeted site, with minimum obstacles to tissue uptake and improved pharmacokinetics and pharmacodynamics. Considering these advantages, several liposome-based strategies are already approved for clinical trials [35]. However, most of these strategies are based on single-agent delivery, which still faces some of the limitations associated with free drugs such as high therapeutic concentration and thus drug resistance. Therefore, in this study, we have prepared a nanoliposome system which encapsulates two drugs, celecoxib, and genistein, either alone or together in the desired ratio. These nanoliposomes were imaged under TEM (Fig. 1), which suggest that the morphology of EL (A), CL (B), GL (C), and CGL (D) varies from spherical to quasi-spherical with average particle size distribution 110, 90, 90, and 85 nm, respectively (inset). The TEM image of CGL clearly shows a dense layer at the surface, which could be ascribed to the lipid layer, however, the amorphous core could be due to the encapsulated drugs. The average particle size distribution pattern advocates that the incorporation of celecoxib and genistein drugs offers a decrease in the size of CGL, which could be due to the improved complexation of drugs with the components of the liposomes. The hydrodynamic diameter of above-prepared nanoliposomes dispersed in PBS (E) and water (F) was also investigated. The hydrodynamic size of EL, CL, GL, and CGL was found to be 112, 108, 98, and 92 nm, which matches well with the diameter trend obtained from TEM image. The minor increase in diameter could be due to the hydrodynamics of nanoliposomes dispersed in PBS. Further, the nanoliposomes were also dispersed in water and their stability was monitored by following the variation in their hydrodynamic size. As expected, there was no significant change in the hydrodynamic size of nanoliposomes when compared with the nanoliposomes dispersed in PBS. Additionally, the zeta potential measurement of PBS dispersed nanoliposomes showed nearly zero values (a range between −2.0 and −0.6 mV), whereas, water dispersed nanoliposomes showed high negative values (−50 to −46 mV). Fig. 1G represents a schematic diagram of a possible arrangement of PEG, celecoxib, and genistein in prepared nanoliposomes. It is expected that both the drugs are entrapped in the hydrophobic core of the nanoliposomes.

The loading of celecoxib and genistein drugs within nanoliposomes was quantified by monitoring the absorbance intensity at 255 and 382 nm, respectively. Free drugs, not encapsulated in nanoliposomes, were removed using 10 kDa Amicon tubes centrifuged at 4000 rpm. The so obtained purified nanoliposomes were disrupted by chloroform and methanol, which released out the drug/s from the nanoliposomes. The quantification of each drug encapsulated within the liposomes was calculated from the standard curve of celecoxib or genistein ranging from 10 μg–100 μg/mL. The quantification results suggest that ~91.7% celecoxib is encapsulated in CL, whereas, GL showed ~68.9% of genistein loading (Fig. 2A). However, the encapsulation of celecoxib and genistein in CGL was found to be 78.7 and 63.5%, respectively. Further, the celecoxib and genistein release kinetics (Fig. 2B) from CGL revealed almost similar release pattern in 10 mM glutathione medium over 50 h. This observation suggests that a constant concentration of both the drugs could be maintained for a longer period when a desired ratio of drugs is encapsulated in nanoliposome form.

3.2. Nanoliposomes encapsulating celecoxib and genistein induce cell death in prostate cancer cells but not to the fibroblasts

One of the major reasons for the development of drug resistance and side effects associated with the use of anticancer agents is the requirement of high concentration of the drug. It is well established that mechanistically anticancer drugs induce the blockage of the signaling pathways needed for cancer cell proliferation. In this context, it becomes vital that if multiple drugs are combined together, need much lesser concentration to produce the desired efficacy than individual drugs because multiple drugs could target multiple key pathways to inhibit the progression of cancer cells. Therefore, to demonstrate that the developed CGL formulation selectively inhibits the cancer cell proliferation, we used two prostate cancer cell culture models, PC-3 and LNCaP, and followed the cell viability using MTT assay (Fig. 3). As clearly evident from Fig. 3 that CL and GL induce ~20–22% decrease in cell viability of PC-3 cells, however, CGL induced ~75% decrease in viability when exposed to for 24 h (A). Further incubation of CL and GL to PC-3 cells for 48 (B) and 72 (C) hrs did not induce any significant improvement in cell viability inhibition. Interestingly, 72 h exposure of CGL to PC-3 cells lead to ~85% decrease in cell viability suggesting that the combined effect of celecoxib and genistein is improved over a longer period of time. Considering the release kinetics of celecoxib and genistein from CGL, it can be concluded that both of these drugs maintain sufficient concentrations in the glutathione medium which is enough to inhibit the PC-3 cells viability. We also investigated the effect of CL, GL, and CGL on LNCaP (Fig. 3D, E, and F). Although 24 h exposure of CGL induced ~60% decrease in cell proliferation but the CL and GL exposure could lead to only ~20% decrease. The exposure of Cl, GL, and CGL for 48 and 72 h did not show any significant improvement in the decrease of LNCaP cell viability than 24 h exposure. This observation suggests that the CGL formulation is more effective in PC-3 cells than LNCaP. This effect can be explained by considering the fact that PC-3 and LNCaP cell lines show some fundamental differences,

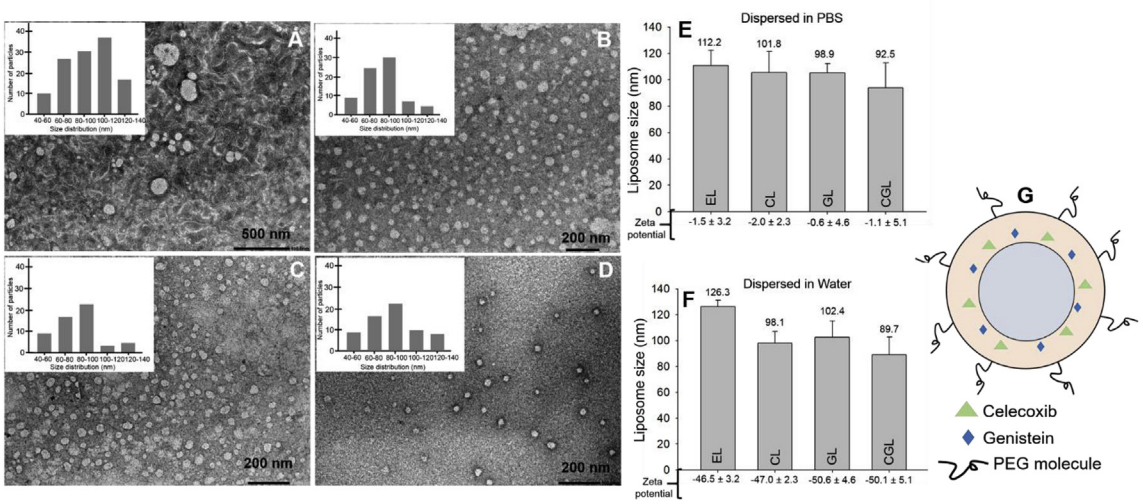

Fig. 1. Study of shape, size and hydrodynamic diameter of nanoliposomes containing celecoxib, genistein and both celecoxib and genistein drugs. TEM image of EL (A), CL (B), GL (C), and CGL (D) drugs containing liposomes, inset shows the average diameter of liposomes. Hydrodynamic diameter and zeta potential of EL, CL, G, and CGL dispersed in PBS (E) and water (F). Data represent the average and standard deviation calculated from the three independent experiments. A schematic diagram predicting the possible location of celecoxib and genistein drugs within the liposomes (G).

such as former are androgen-insensitive while latter are androgen-sensitive. Further, this sensitivity has been well co-related with the expression of Glut protein expression levels in the literature [36]. The insensitive cell lines (PC-3) are shown to express more Glut-1 receptors than insensitive (LNCaP) cells. Since our nanoliposomal formulation contains Genistein (an inhibitor of Glut protein expression), the high Glut-1 protein expression cells (PC-3) were more affected than low expression LNCaP cells. Further, we also investigated the effect of CL, GL, and CGL on the proliferation of fibroblast cells (Fig. 3G, H, and I). As expected, these formulations did not show any significant decrease in cell viability. Although CGL showed a minor decrease in cell viability (< 10%) but at extended (48, and 72) hrs of exposure.

3.3. Metastatic potential of prostate cancer cells is inhibited by nanoliposomes encapsulating celecoxib and genistein

Cancer metastasis is predominantly controlled by migration and invasion potential of tumor cells [37,38]. It is reported that PC-3 cells exhibit highly metastatic potential [39]. Therefore, to evaluate the effect of CGL over the migration capacity of PC-3 cells, we performed the well-known wound healing assay. As clearly depicted in Fig. 4, the healing of wound was quick when exposed to EL for 0 (A), 24 (E), and 48 (I) hrs, suggesting that the components of nanoliposomes do not exert any inhibition to normal wound healing process. Further, exposure of CL to wound revealed that the healing was slow for 0 (B) and 24 (F) hrs but after 48 h (J) the healing was almost as similar as EL. This trend of wound healing suggests that the effect of celecoxib was only for 24 h and became ineffective during the later exposure time. Exposure of wound to GL for 0 (C), 24 (G) and 48 (K) hrs showed persistent inhibition of healing potential of PC-3 cells at all the time points. However, it can be seen that at 24 h of exposure, cells did show some healing, similar to CL, but at 48 h, increase in cell population was observed while the wound area remains to widen. Interestingly, when CGL was exposed to the wound, clear inhibition of migration of PC-3 cells towards wound area was observed at all the time points, 0 (D), 24 (H), and 48 (L) hrs. It can also be seen that the cell population in the nearby area of the wound is decreased after 24, and 48 h of exposure. Additionally, at 48 h, it is clearly seen that cells are of spherical morphology, suggesting dead cells. Thus, from the migration assay, it can be concluded that CL and GL are effective for short-term inhibition of metastatic capacity of PC-3 cells, however, the combination of celecoxib and genistein (CGL) may lead to long-term suppression of PC-3 cells in vitro.

3.4. Investigation of the levels of cellular markers in PC-3 cells

It is well established with most of the drug-mediated anticancer activity involves the activation of mechanisms which lead to the generation of reactive oxygen species in cancer cell cytoplasm. It has been reported that cancer cells are more sensitive than normal cells to the cellular accumulation of excessive ROS [40–42]. This opportunity window has been exploited to create novel strategies to selectively kill cancer cells without affecting normal cells. For example, use of paclitaxel has been reported to impart anticancer activity by enhancing the production of ROS by nitric oxide synthase activation [43,44]. Similarly, celecoxib drug is also reported to modulate the ROS levels in PC-

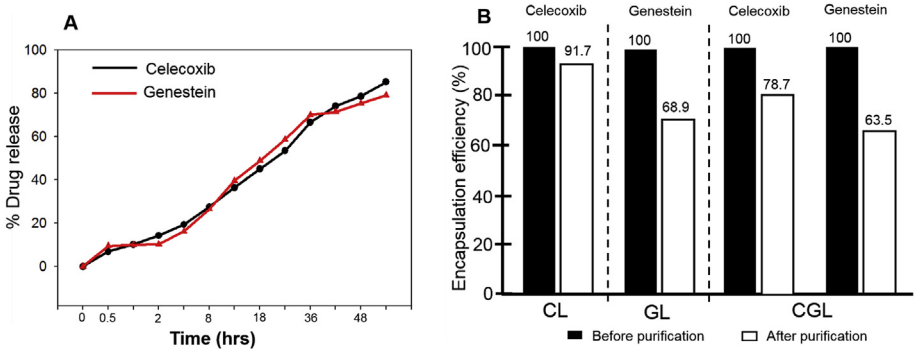

Fig. 2. Drug release profile and stability of nanoliposomes. Nanoliposomes containing celecoxib alone (CL), genistein alone (GL), or the combination (CGL), celecoxib encapsulation alone was ~91.7%, genistein encapsulation alone was ~68.9%, and the encapsulation of both agents was ~78.7% and ~63.5%, respectively (A). Data represent averages of at least three independent experiments. Drug release kinetics of celecoxib and genistein from CGL showed ~82% of celecoxib and 79% of genistein was released from CGL over 48 h in 10 mM glutathione medium. Data represent averages of at least three independent experiments (B).

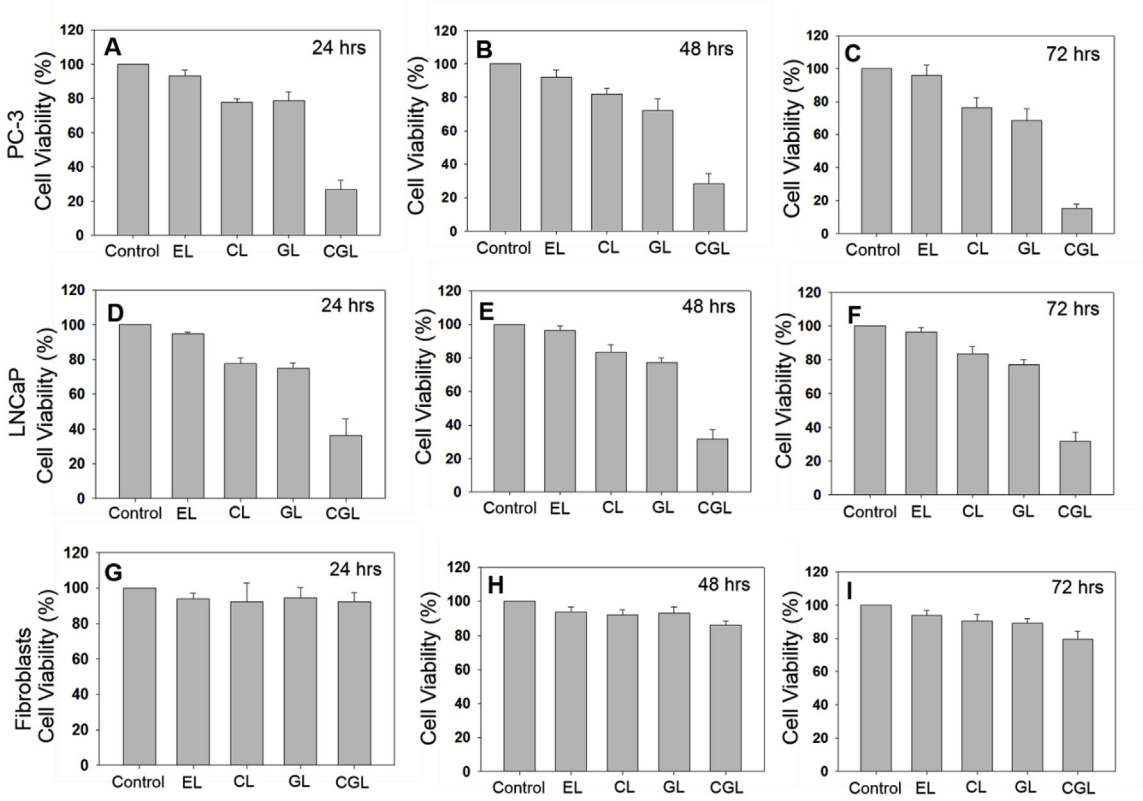

Fig. 3. Comparison of efficacy of CGL with the individual drugs and empty liposomes in prostate cancer cell culture models. The different nanoliposomal formulations were exposed to PC-3 cells for 24 (A), 48 (B), and 72 (C) hrs, LNCaP cells for 24 (D), 48 (E), and 72 (F) hrs, and Fibroblasts cells for 24 (G), 48 (H), and 72 (I) hrs. Data represent averages of at least three independent experiments; bars represent standard deviation.

3 cells to induce apoptosis by the COX pathway [25,45]. Therefore, we also investigated the level of free radicals after the exposure of our nanoliposome formulations to prostate cancer cells. As it is clearly evident from Fig. 5, the exposure of EL, CL, and GL did not induce much of ROS generation in PC-3 cells, however, cells exposed to CGL leads to the significant (3 folds) production of ROS (Fig. 5A). This observation suggests that PC-3 cells exposed to the combination of celecoxib and genistein lead to the activation of signaling pathways which induce the high production of ROS. Further, these excessive ROS level cause damage to the PC-3 cells, as observed by our cell viability data. Next, we also studied that ROS levels in LNCaP cells exposed to different nanoliposomes. Data from Fig. 5B indicate that the trend of ROS production was similar to PC-3 cells, however, the amount of ROS produced due to CGL exposure to LNCaP cells was much lower (~1.6 folds) than PC-3 cells (~3 folds). Considering our data with cell viability assay, the developed CGL formulation showed better inhibition to PC-3 cells than LNCaP, which is in agreement with our ROS generation data, suggesting that ROS play a major role in CGL mediated killing of prostate cancer cells. Additionally, we also studied the effect of these nanoliposomes over the normal cells, considering fibroblasts as in vitro model system (Fig. 5C). The results showed that EL, CL, GL, and CGL did not induce any significant enhancement in ROS generation in

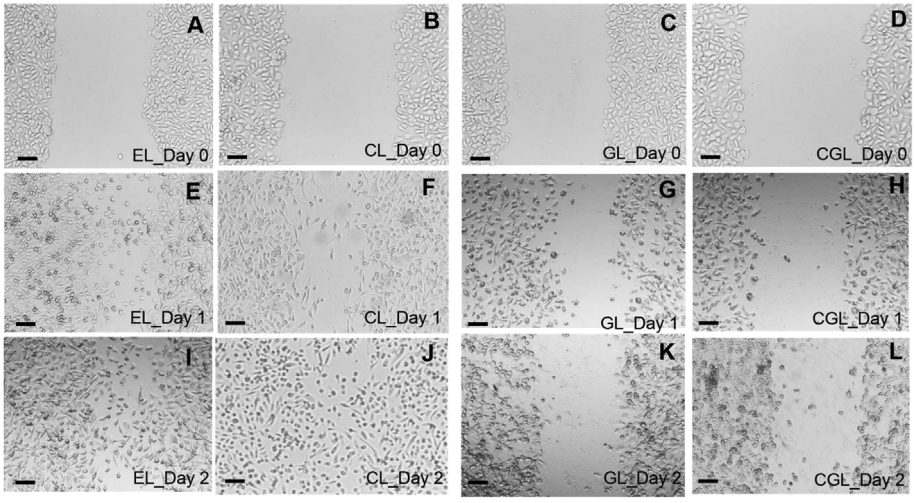

Fig. 4. CGL reduce prostate cancer cells migration in vitro. Wound/scratch created PC-3 cells were exposed to EL, CL, GL, and CGL for 48 h and the microscopic (100X) pictures were captured at day 0 (A, B, C, D), 1 (E, F, G, H), and 2 (I, J, K, L) and wound closure was analysed.

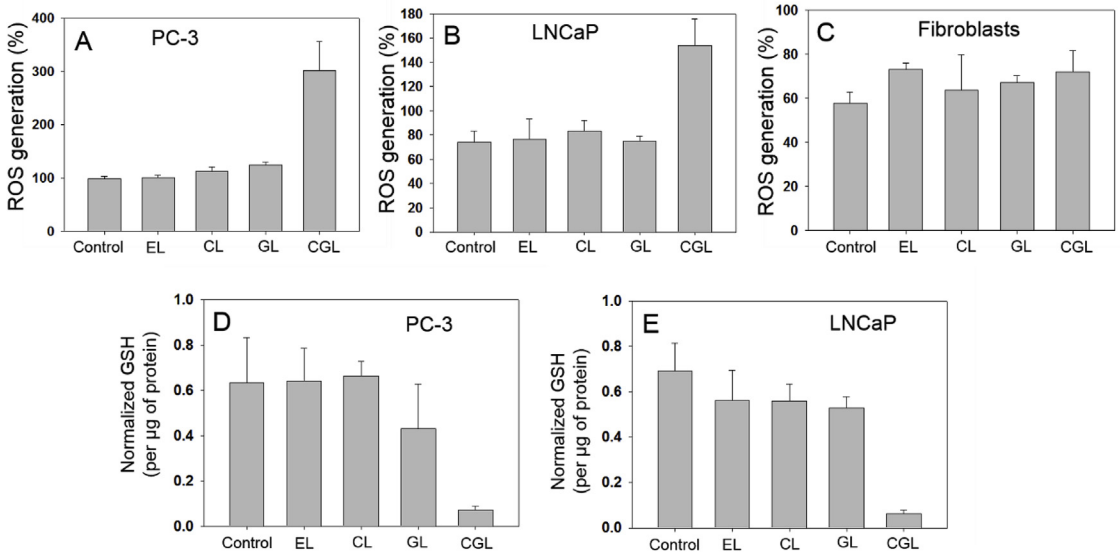

Fig. 5. Estimation of ROS generation and GSH levels in prostate cancer cells. CL, GL, and CGL can efficiently induce the ROS generated inside PC-3 (A), LNCaP (B) but not in Fibroblasts (C). The intracellular level of GSH was also estimated after the 24 h exposure of CL, GL, and CGL in PC-3 (D), LNCaP (E), and Fibroblasts (F) cells. Data expressed as standard error (SE) calculated from three (n = 3) independent experiments.

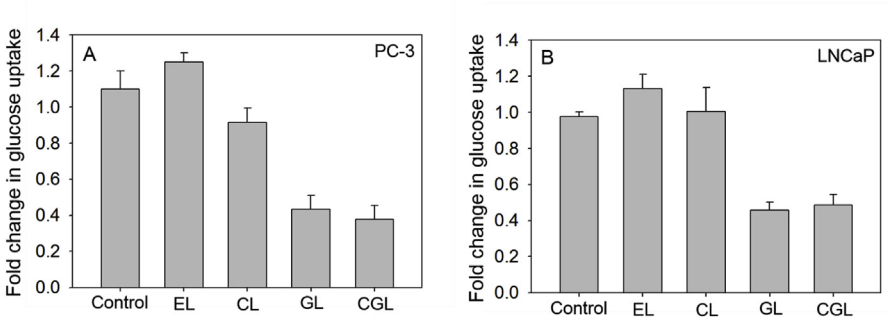

Fig. 6. Estimation of glucose uptake in prostate cancer cells. The glucose uptake assay was monitored by recording fluorescence intensity of NBDG uptake in flow cytometer after exposure of CL, GL, and CGL to PC-3 (A), and LNCaP (B) cells. Data expressed as standard error (SE) calculated from three (n = 3) independent experiments.

fibroblasts compared to untreated cells. This observation suggests that lower concentrations of celecoxib and genistein did not induce any significant inhibition in either prostate cancer cells or normal fibroblasts cells, however, when combined together (in CGL), cause significant killing to prostate cancer cells but not to fibroblasts cells. This could be further hypothesized that the CGL target selective signaling pathways expressed in cancer cells but not in normal cells, which lead to this targeted action of our anticancer formulation. Singh et al. have reported that the inhibition of drug resistance and induction of apoptosis in skin cancer model when a mixture of doxorubicin and celecoxib was combined in a liposome form. This formulation showed excellent anticancer activity compared to individually encapsulated liposomes due to the better inhibition of key proteins (AKT and COX-2), overexpressed in melanoma, thus offering synergistic inhibit multiple key signaling pathways [24].

Glutathione (GSH), is one of the prominent cellular thiol molecules, which plays a major role in redox balance in the cytoplasm, which is critical to cellular ROS, cell growth, cell signaling, proliferation, differentiation, and apoptosis [46]. Therefore, we also estimated the alteration in cellular GSH levels in response to CGL treatment of prostate cancer cells (Fig. 5D and E). As evident from the data, PC-3 cells exposed to EL, and CL did not show any significant increase or decrease in GSH levels with respect to untreated control cells (Fig. 5D). However, PC-3 cells exposed to GL and CGL undergo ~30% and ~90%, respectively drop in GSH synthesis in cells, suggesting that CGL also inhibits the GSH synthesis mechanism of cells, which could lead to the high ROS production in cells. Additionally, LNCaP cells showed ~10% decrease in GSH production when exposed to EL, CL, and GL, whereas CGL exposure leads to ~90% decrease (Fig. 5E). We also extended the investigation of changes in GSH levels after EL, CL, and GL, and CGL treatment to fibroblasts cells. As expected, fibroblasts cells did not show any significant drop in cellular GSH concentration even after the treatment of nanoliposomal formulations (Fig. 5F). Therefore, it can be concluded that CGL offers similar levels of decrease in GSH synthesis in cells, however, LNCaP cells are more tolerant to cellular GSH and hence ROS production is limited than PC-3 cells.

Glut-1 proteins are present in the plasma membrane of mammalian cells, which play important role in the transport of glucose across the cell. In cancer cells, to meet the high metabolism, Glut-1 proteins facilitate the rapid transport of glucose. Due to this need, cancer cells have adapted to overexpress the Glut-1 receptors on their cell membrane, and this has also correlated with poor survival of patients in human studies [18]. Considering this, we investigated the levels of glucose transport in PC-3 (Fig. 6A) and LNCaP (Fig. 6B) cells. The obtained data suggest that in both the cell lines the transport of glucose was inhibited for about 60% when exposed to GL and CGL. It must be mentioned here that both of these cell lines are reported to overexpress the Glut-1 receptors, but to different extent, which facilitate the glucose transport. It is reported that PC-3 cells show more Glut-1 receptor expression than LNCaP, however, we observed a similar pattern of decrease of glucose uptake in both of these cell lines. This could be due to the fact that the release genistein from nanoliposomes is present in excess and therefore, it would inhibit the Glut-1 receptors in similar extent to both the cell lines. Thus, it does not really correlate with the

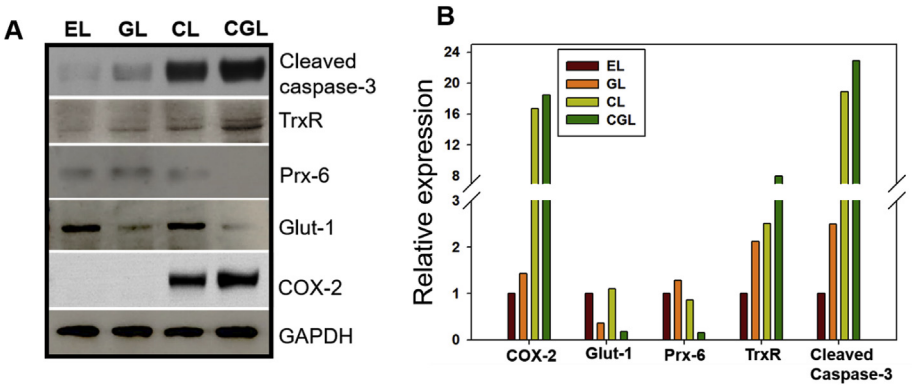

Fig. 7. Expression level of antioxidant proteins analysis by western blotting in PC-3 cells. The protein involved in maintaining cellular antioxidant system (TrxR, Prx-6, Glut-1, COX-2, and caspase-3) were monitored by western blotting (A). The corresponding densitometry analysis of expressed proteins were normalized to GAPDH and expressed in fold change (B).

number of Glut-1 receptors present on the cell surface, which subsequently results into a similar pattern of glucose uptake in PC-3 and LNCaP cells. Additionally, genistein is a well-known inhibitor of Glut-1 receptors, while celecoxib is not.

Therefore, it can be concluded that due to the low glucose uptake, the metabolism of PC-3 and LNCaP cells might have significantly decreased and simultaneously celecoxib inhibits the COX-2 pathway. Both of these events simultaneously imparting the inhibition of prostate cancer cells.

3.5. Nanoliposomes encapsulating celecoxib and genistein oversee the expression of key signaling pathways to inhibit the growth of prostate cancer cells

Considering our selected anticancer agents, celecoxib, and genistein, for the preparation of CGL, we investigated the expression of COX-2 and Glut-1 proteins (Fig. 7A and B). It was expected that inhibition of two key processes, the COX-2 pathway (by celecoxib) and Glut-1 protein expression (by Genistein), the proliferation of prostate cancer cells can be inhibited. Surprisingly, in our investigation, the expression of COX-2 was significantly increased in PC-3 cells when exposed to CL and CGL. This trend could be attributed due to the inhibition of COX-2 signaling pathway by celecoxib drug, which in turn increases the COX-2 protein level but this is purely hypothetical. Such trend has been reported by several groups and suggests that although binding of celecoxib to COX-2 leads to the inhibition of COX activity, there is a compensatory increase in corresponding protein expression to alleviate the inhibition [47–49]. Genistein is well known to inhibit the expression of Glut-1 receptors, therefore, in our investigation too, we observed that the expression of Glut-1 was unaffected when PC-3 cells are exposed with EL, and CL, however, GL, and CGL exposure leads to the significant decrease (~90%) of Glut-1 protein expression. Further, the decrease in Glut-1 protein expression was more in cells treated with CGL than GL (specific inhibitor). This could be due to the combination effect of celecoxib and genistein (from CGL), where former can also have some non-specific inhibitory effect on Glut-1 receptors along with the specific inhibitor genistein, therefore, we observe better Glut-1 receptor inhibition after CGL treatment. This observation further translates into the cell viability results, which shows better cell growth inhibition when used CGL. Thus, this observation suggests that Glut-1 inhibition could have decreased the glucose uptake in PC-3 cells, thus inhibition to the cell proliferation. Since, we observed that (Fig. 5A, and B) exposure of CL, GL and CGL to prostate cancer cells leads to the generation of excessive ROS, we also investigated the expression of proteins involved in the oxidative stress defense, thioredoxin reductase (TrxR) and peroxiredoxin-6 (Prx-6). The expression level of Prx-6 decreases significantly upon exposure to CGL. Since unlike other Prxs (1–5), Prx-6 uses GSH as a physiological reluctant, therefore, it is expected that the expression of Prx-6 would be controlled by cellular GSH [46,50,51]. As our GSH expression results also revealed that after CGL treatment the GSH level decreases significantly, thus the level of Prx-6 must also decrease. Additionally, TrxR was also considered as a general marker for cellular oxidative stress. TrxR is a selenoprotein, containing a C-terminus cysteine-selenocysteine redox pair, involved in regulating the redox status of (oxidized/reduced environment) of the cells [52,53]. As expected, PC-3 cells exposed to CL, GL, and CGL triggered an increase in TrxR protein expression compared to EL treated cells. Among them, CGL induced ~8 fold increase in TrxR expression than CL (~2 fold), and GL (2.3 fold). The observed trend is in agreement with the ROS generation in PC-3 cells (Fig. 5A). Further, in order to establish the prostate cancer cells death due to apoptosis, we studied the expression of cleaved caspase-3. As expected, the cleaved caspase-3 expression was significantly increased in PC-3 cells exposed to CL (20 fold), and CGL (23 fold). This observation suggests that CGL exposure leads to the induction of apoptosis in prostate cancer cells.

Additionally, mRNA expressions for COX-2, Glut-1, Prx-6, PrxR, and cleaved caspases-3 in PC-3 cells exposed to EL, CL, GL, and CGL was also studied (Fig. 8). The results show that COX-2 mRNA expression decreases significantly when PC-3 cells are exposed to CL, GL, and CGL, suggesting that celecoxib inhibits the COX-2 pathway (Fig. 8A). Considering the western blotting data, where CL and CGL induce the high expression of the COX-2 protein, it can be suggested that although new COX-2 proteins are not synthesized, however, the synthesized proteins are not degraded. Further, the mRNA expression of the Glut-1 protein was investigated (Fig. 8B), results show that GL and CGL significantly inhibit the mRNA synthesis. This observation is in agreement with our western blot data. Further, it was surprising to observe that CL exposure also inhibits the mRNA synthesis of Glut-1. It has been reported that in endometrial cancer the expression of COX-2 and Glut-1 are strongly correlated [54]. The mRNA expression of Prx-6 showed an increase of the synthesis on PC-3 cells exposed to CL, GL, and CGL, suggesting the inverse correlation with cellular GSH concentration (Fig. 8C). This observation could be ascribed due to the absence of functional Prx-6 protein, in absence of GSH, which may act as a trigger to synthesize more Prx-6 mRNA. Considering the enhanced ROS level in PC-3 cells upon CL, GL, and CGL exposure, the mRNA of TrxR is expected to increase (Fig. 8D). Thus, this observation is in agreement with our results of ROS and western blotting data. Further, to support the observation in western blotting data, we also investigated the mRNA synthesis of cleaved caspase-3. The data suggest that there was a significant increase in mRNA level in PC-3 cells exposed to CL, GL, and CGL (Fig. 8E). The highest expression in CGL exposed PC-3 cells suggests that this formulation was able to induce the maximum apoptosis. Considering our cell proliferation data it can be concluded that since CL and GL could also impart little inhibition to PC-3 and LNCaP cells proliferation, a similar trend was also observed in mRNA expression.

4. Conclusion

In this study, we have developed celecoxib and genistein

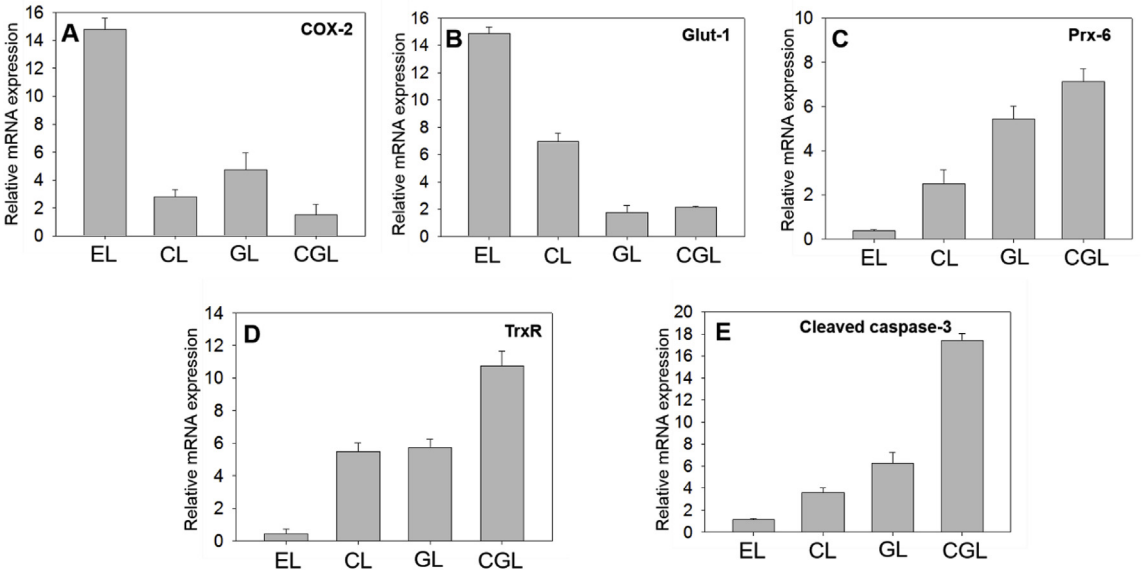

Fig. 8. Expression level of antioxidant genes in PC-3 cells after the treatment of CL, GL, and CGL. Gene (TrxR, Prx-6, Glut-1, COX-2, and caspase-3) expression level was plotted as fold change and normalized with gapdh gene expression level. Data reported as standard error (SE) calculated from three (n = 3) independent experiments.

encapsulating nanoliposomes, which represent a unique class of anticancer agent with the potential of being used to treat several types of cancer including prostate. The prepared nanoliposomes are ~100 nm in diameter, which is considered as preferred size to be readily internalized by cancer cells. The encapsulated drugs, celecoxib, and genistein retain their anticancer properties and in fact, work synergistically to decrease the proliferation of prostate cancer cells. In this context, it may be argued that the similar release kinetic profile of both of these drugs could facilitate the optimum concentration at the targeted site. Although the CGL could inhibit the prostate cancer cell proliferation up to 90%, whereas this formulation was not any significant toxicity to normal fibroblast cells, suggesting that the concentration of celecoxib and genistein needed to kill prostate cancer cells is non-toxic to normal cells. The migration and invasion property of prostate cancer cells was also observed to be completely inhibited by the CGL formulation. Mechanistically, it was found that the nanoliposomal formulation containing a combination of celecoxib and genistein drugs could induce the ROS generation, a significant decrease in cellular GSH concentration, and inhibition of glucose uptake. Taken together, these events successfully inhibit the proliferation of prostate cancer cells. The proteomic analysis of multiple pathways suggests that inhibition of COX-2 signaling pathway, decrease in Glut-1 proteins, decrease in Prx-6 proteins, and increase in TrxR and caspase-3 levels. Further, considering the results of mRNA expression of these proteins suggest that collectively these events negatively regulate the cell proliferation of prostate cancer cells. On the basis of the observed results, it can be concluded that the combination of celecoxib and genistein offer a unique mechanism of action by simultaneously targeting several key pathways essential for the development of prostate cancer cells. Although the developed nanoliposomes exhibited excellent in vitro results and thus hold potential to be developed further for cancer treatment applications, more comprehensive studies are needed to realize the full potential of this formulation for the management of prostate and other cancer types.

Conflicts of interest

Authors declare no conflict of interest.

Acknowledgement

Authors acknowledge Jilin University. China for the necessary support and facility to carry out this project.

References

[1] M.C. Wong, W.B. Goggins, H.H. Wang, F.D. Fung, C. Leung, S.Y. Wong, C.F. Ng, J.J. Sung, Global incidence and mortality for prostate cancer: analysis of temporal patterns and trends in 36 countries, Eur. Urol. 70 (2016) 862–874.
[2] E.T. Hawk, J.L. Viner, A. Dannenberg, R.N. DuBois, COX-2 in cancer–a player that's defining the rules, J. Natl. Cancer Inst. 94 (2002) 545–546.
[3] N. Ghosh, R. Chaki, V. Mandal, S.C. Mandal, COX-2 as a target for cancer chemotherapy, Pharmacol. Rep. 62 (2010) 233–244.
[4] S. Gupta, M. Srivastava, N. Ahmad, D.G. Bostwick, H. Mukhtar, Over-expression of cyclooxygenase-2 in human prostate adenocarcinoma, Prostate 42 (2000) 73–78.
[5] R. Yoshimura, H. Sano, C. Masuda, M. Kawamura, Y. Tsubouchi, J. Chargui, N. Yoshimura, T. Hla, S. Wada, Expression of cyclooxygenase-2 in prostate carcinoma, Cancer 89 (2000) 589–596.
[6] S. Zha, W.R. Gage, J. Sauvageot, E.A. Saria, M.J. Putzi, C.M. Ewing, D.A. Faith, W.G. Nelson, A.M. De Marzo, W.B. Isaacs, Cyclooxygenase-2 is up-regulated in proliferative inflammatory atrophy of the prostate, but not in prostate carcinoma, Cancer Res. 61 (2001) 8617–8623.
[7] T. Etheridge, J. Liou, T.M. Downs, E.J. Abel, K.A. Richards, D.F. Jarrard, The impact of celecoxib on outcomes in advanced prostate cancer patients undergoing androgen deprivation therapy, Am J Clin Exp Urol 6 (2018) 123–132.
[8] R. Garg, J.M. Blando, C.J. Perez, P. Lal, M.D. Feldman, E.M. Smyth, E. Ricciotti, T. Grosser, F. Benavides, M.G. Kazanietz, COX-2 mediates pro-tumorigenic effects of PKCepsilon in prostate cancer, Oncogene 8-37 (34) (2018) 4735–4749.
[9] S.K. Singh, J.W. Lillard Jr., R. Singh, Reversal of drug resistance by planetary ball milled (PBM) nanoparticle loaded with resveratrol and docetaxel in prostate cancer, Cancer Lett. 427 (2018) 49–62.
[10] A. Greenhough, H.J. Smartt, A.E. Moore, H.R. Roberts, A.C. Williams, C. Paraskeva, A. Kaidi, The COX-2/PGE2 pathway: key roles in the hallmarks of cancer and adaptation to the tumour microenvironment, Carcinogenesis 30 (2009) 377–386.
[11] E.R. Greene, S. Huang, C.N. Serhan, D. Panigrahy, Regulation of inflammation in cancer by eicosanoids, Prostag. Other Lipid Mediat. 96 (2011) 27–36.
[12] R. Nachat-Kappes, A. Pinel, K. Combe, B. Lamas, M.C. Farges, A. Rossary, N. Goncalves-Mendes, F. Caldefie-Chezet, M.P. Vasson, S. Basu, Effects of enriched environment on COX-2, leptin and eicosanoids in a mouse model of breast cancer, PLoS One 7 (2012) e51525.
[13] X. Zheng, X.X. Cui, Z. Gao, Y. Zhao, Y. Lin, W.J. Shih, M.T. Huang, Y. Liu, A. Rabson, B. Reddy, C.S. Yang, A.H. Conney, Atorvastatin and celecoxib in combination inhibits the progression of androgen-dependent LNCaP xenograft prostate tumors to androgen independence, Cancer Prev. Res. 3 (2010) 114–124.
[14] L. Gong, C.F. Thorn, M.M. Bertagnolli, T. Grosser, R.B. Altman, T.E. Klein, Celecoxib pathways: pharmacokinetics and pharmacodynamics, Pharmacogenetics Genom. 22 (2012) 310–318.
[15] T. Grosser, S. Fries, G.A. FitzGerald, Biological basis for the cardiovascular consequences of COX-2 inhibition: therapeutic challenges and opportunities, J. Clin. Invest. 116 (2006) 4–15.

[16] F.E. Silverstein, G. Faich, J.L. Goldstein, L.S. Simon, T. Pincus, A. Whelton, R. Makuch, G. Eisen, N.M. Agrawal, W.F. Stenson, A.M. Burr, W.W. Zhao, J.D. Kent, J.B. Lefkowith, K.M. Verburg, G.S. Geis, Gastrointestinal toxicity with celecoxib vs nonsteroidal anti-inflammatory drugs for osteoarthritis and rheumatoid arthritis: the CLASS study: a randomized controlled trial. Celecoxib Long-term Arthritis Safety Study, J. Am. Med. Assoc. 284 (2000) 1247–1255.
[17] S. Singh, Glucose decorated gold nanoclusters: a membrane potential independent fluorescence probe for rapid identification of cancer cells expressing Glut receptors, Colloids Surfaces B Biointerfaces 155 (2017) 25–34.
[18] M.L. Macheda, S. Rogers, J.D. Best, Molecular and cellular regulation of glucose transporter (GLUT) proteins in cancer, J. Cell. Physiol. 202 (2005) 654–662.
[19] J.D. Chandler, E.D. Williams, J.L. Slavin, J.D. Best, S. Rogers, Expression and localization of GLUT1 and GLUT12 in prostate carcinoma, Cancer 97 (2003) 2035–2042.
[20] J.T. Hwang, J. Ha, O.J. Park, Combination of 5-fluorouracil and genistein induces apoptosis synergistically in chemo-resistant cancer cells through the modulation of AMPK and COX-2 signaling pathways, Biochem. Biophys. Res. Commun. 332 (2005) 433–440.
[21] C. Ma, A.W. Armstrong, Severe adverse events from the treatment of advanced melanoma: a systematic review of severe side effects associated with ipilimumab, vemurafenib, interferon alfa-2b, dacarbazine and interleukin-2, J. Dermatol. Treat. 25 (2014) 401–408.
[22] C. Demetzos, N. Pippa, Advanced drug delivery nanosystems (aDDnSs): a mini-review, Drug Deliv. 21 (2014) 250–257.
[23] D. Shah, R. Savaliya, P. Patel, K. Kansara, A. Pandya, A. Dhawan, S. Singh, Curcumin Ag nanoconjugates for improved therapeutic effects in cancer, Int. J. Nanomed. 13 (2018) 75–77.
[24] S. Singh, Liposome encapsulation of doxorubicin and celecoxib in combination inhibits progression of human skin cancer cells, Int. J. Nanomed. 13 (2018) 11–13.
[25] R. Gowda, G. Kardos, A. Sharma, S. Singh, G.P. Robertson, Nanoparticle-based celecoxib and plumbagin for the synergistic treatment of melanoma, Mol. Canc. Therapeut. 16 (2017) 440–452.
[26] R. Savaliya, P. Singh, S. Singh, Pharmacological drug delivery strategies for improved therapeutic effects: recent advances, Curr. Pharmaceut. Des. 22 (2016) 1506–1520.
[27] J. Fang, T. Sawa, H. Maeda, Factors and mechanism of "EPR" effect and the enhanced antitumor effects of macromolecular drugs including SMANCS, Adv. Exp. Med. Biol. 519 (2003) 29–49.
[28] M.L. Zhu, X.L. Xu, X.J. Wang, N.N. Zhang, K.J. Lu, J. Qi, F.Y. Jin, D. Liu, Y.Z. Du, Sialic-acid-anchored micelles: a hierarchical targeting device for enhanced tumor tissue accumulation and cellular internalization, Mol. Pharm. 28-15 (9) (2018) 4235–4246.
[29] N. Desai, V. Trieu, Z. Yao, L. Louie, S. Ci, A. Yang, C. Tao, T. De, B. Beals, D. Dykes, P. Noker, R. Yao, E. Labao, M. Hawkins, P. Soon-Shiong, Increased antitumor activity, intratumor paclitaxel concentrations, and endothelial cell transport of cremophor-free, albumin-bound paclitaxel, ABI-007, compared with cremophor-based paclitaxel, Clin. Canc. Res. 12 (2006) 1317–1324.
[30] E. Huynh, G. Zheng, Cancer nanomedicine: addressing the dark side of the enhanced permeability and retention effect, Nanomedicine 10 (2015) 1993–1995.
[31] S.K. Golombek, J.N. May, B. Theek, L. Appold, N. Drude, F. Kiessling, T. Lammers, Tumor targeting via EPR: strategies to enhance patient responses, Adv. Drug Deliv. Rev. 31-130 (2018) 17–38.
[32] Y. Patil, H. Shmeeda, Y. Amitay, P. Ohana, S. Kumar, A. Gabizon, Targeting of folate-conjugated liposomes with co-entrapped drugs to prostate cancer cells via prostate-specific membrane antigen (PSMA), Nanomedicine 14 (2018) 1407–1416.
[33] Y. Patil, Y. Amitay, P. Ohana, H. Shmeeda, A. Gabizon, Targeting of pegylated liposomal mitomycin-C prodrug to the folate receptor of cancer cells: intracellular activation and enhanced cytotoxicity, J. Contr. Release 225 (2016) 87–95.
[34] K.N. Panagiotaki, Z. Sideratou, S.A. Vlahopoulos, M. Paravatou-Petsotas, M. Zachariadis, N. Khoury, V. Zoumpourlis, D. Tsiourvas, A triphenylphosphonium-functionalized mitochondriotropic nanocarrier for efficient Co-delivery of doxorubicin and chloroquine and enhanced antineoplastic activity, Pharmaceuticals 10 (2017).
[35] H.I. Chang, M.K. Yeh, Clinical development of liposome-based drugs: formulation, characterization, and therapeutic efficacy, Int. J. Nanomed. 7 (2012) 49–60.
[36] P. Gonzalez-Menendez, D. Hevia, A. Rodriguez-Garcia, J.C. Mayo, R.M. Sainz, Regulation of GLUT transporters by flavonoids in androgen-sensitive and -insensitive prostate cancer cells, Endocrinology 155 (2014) 3238–3250.
[37] P. Friedl, K. Wolf, Tumour-cell invasion and migration: diversity and escape mechanisms, Nat. Rev. Canc. 3 (2003) 362–374.
[38] J.J. Bravo-Cordero, L. Hodgson, J. Condeelis, Directed cell invasion and migration during metastasis, Curr. Opin. Cell Biol. 24 (2012) 277–283.
[39] S. Tai, Y. Sun, J.M. Squires, H. Zhang, W.K. Oh, C.Z. Liang, J. Huang, PC3 is a cell line characteristic of prostatic small cell carcinoma, Prostate 71 (2011) 1668–1679.
[40] M. Diehn, R.W. Cho, N.A. Lobo, T. Kalisky, M.J. Dorie, A.N. Kulp, D. Qian, J.S. Lam, L.E. Ailles, M. Wong, B. Joshua, M.J. Kaplan, I. Wapnir, F.M. Dirbas, G. Somlo, C. Garberoglio, B. Paz, J. Shen, S.K. Lau, S.R. Quake, J.M. Brown, I.L. Weissman, M.F. Clarke, Association of reactive oxygen species levels and radioresistance in cancer stem cells, Nature 458 (2009) 780–783.
[41] Y.S. Kim, M.J. Kang, Y.M. Cho, Low production of reactive oxygen species and high DNA repair: mechanism of radioresistance of prostate cancer stem cells, Anticancer Res. 33 (2013) 4469–4474.
[42] L.S. Piao, W. Hur, T.K. Kim, S.W. Hong, S.W. Kim, J.E. Choi, P.S. Sung, M.J. Song, B.C. Lee, D. Hwang, S.K. Yoon, CD133+ liver cancer stem cells modulate radioresistance in human hepatocellular carcinoma, Cancer Lett. 315 (2012) 129–137.
[43] J. Alexandre, Y. Hu, W. Lu, H. Pelicano, P. Huang, Novel action of paclitaxel against cancer cells: bystander effect mediated by reactive oxygen species, Cancer Res. 67 (2007) 3512–3517.
[44] Y. Jin, Z. Lu, K. Ding, J. Li, X. Du, C. Chen, X. Sun, Y. Wu, J. Zhou, J. Pan, Antineoplastic mechanisms of niclosamide in acute myelogenous leukemia stem cells: inactivation of the NF-kappaB pathway and generation of reactive oxygen species, Cancer Res. 70 (2010) 2516–2527.
[45] J. Zhu, X. Song, H.P. Lin, D.C. Young, S. Yan, V.E. Marquez, C.S. Chen, Using cyclooxygenase-2 inhibitors as molecular platforms to develop a new class of apoptosis-inducing agents, J. Natl. Cancer Inst. 94 (2002) 1745–1757.
[46] R. Singh, A.S. Karakoti, W. Self, S. Seal, S. Singh, Redox-sensitive cerium oxide nanoparticles protect human keratinocytes from oxidative stress induced by glutathione depletion, Langmuir 32 (2016) 12202–12211.
[47] R. Gowda, S.V. Madhunapantula, D. Desai, S. Amin, G.P. Robertson, Simultaneous targeting of COX-2 and AKT using selenocoxib-1-GSH to inhibit melanoma, Mol. Canc. Therapeut. 12 (2013) 3–15.
[48] A.R. Munkarah, Z. Genhai, R. Morris, V.V. Baker, G. Deppe, M.P. Diamond, G.M. Saed, Inhibition of paclitaxel-induced apoptosis by the specific COX-2 inhibitor, NS398, in epithelial ovarian cancer cells, Gynecol. Oncol. 88 (2003) 429–433.
[49] H.A. Elrod, P. Yue, F.R. Khuri, S.Y. Sun, Celecoxib antagonizes perifosine's anticancer activity involving a cyclooxygenase-2-dependent mechanism, Mol. Canc. Therapeut. 8 (2009) 2575–2585.
[50] S.G. Rhee, S.W. Kang, T.S. Chang, W. Jeong, K. Kim, Peroxiredoxin, a novel family of peroxidases, IUBMB Life 52 (2001) 35–41.
[51] B. Hofmann, H.J. Hecht, L. Flohe, Peroxiredoxins, Biol Chem 383 (2002) 347–364.
[52] Y.H. Jan, D.E. Heck, J.P. Gray, H. Zheng, R.P. Casillas, D.L. Laskin, J.D. Laskin, Selective targeting of selenocysteine in thioredoxin reductase by the half mustard 2-chloroethyl ethyl sulfide in lung epithelial cells, Chem. Res. Toxicol. 23 (2010) 1045–1053.
[53] M. Srivastava, S. Singh, W.T. Self, Exposure to silver nanoparticles inhibits selenoprotein synthesis and the activity of thioredoxin reductase, Environ. Health Perspect. 120 (2012) 56–61.
[54] X. Ma, Y. Hui, L. Lin, Y. Wu, X. Zhang, P. Liu, Clinical significance of COX-2, GLUT-1 and VEGF expressions in endometrial cancer tissues, Pak J Med Sci 31 (2015) 280–284.